Chapter 3

Defect Chemistry of Bulk CeO_2; Stoichiometric and Non-stoichiometric

3.1 Introduction

Ceria's use as an electrolyte in solid oxide fuel cells is a consequence of its fluorite structure which permits the oxygen ions to move with relative ease. From the discussion in Chapter 1 it seems an important factor in the efficiency of these devices is the migration of the oxygen vacancies. The migration of such vacancies is controlled by a number of factors, such as the activation energy and the clustering with dopants. Computer simulation techniques can provide such information, hence it is an important tool in understanding the mass transport behaviour of ceria at an atomic level.

A perennial problem for defect simulation studies is the direct comparison of results with experimental data. The experiments, in many cases, have been carried out at high defect concentrations, while the simulations at a first instance relate to an ideal solution limit. Hence, the problem of defect - defect interactions must be considered when making comparisons between them. However in the present chapter, comparisons are made with hyperfine experimental data [100, 101, 102, 103] which use very small concentrations of In and Cd dopants in the CeO_2 lattice. Such hyperfine experiments have the advantage of yielding unambiguous binding energies and migration data. However, the specific atomic structure of the defects involved is not always clear. Thus, the experiments can be used in conjuction with the simulations to provide a framework for understanding the defect chemistry of CeO_2.

3.1.1 Summary of experimental techniques

The relevant experimental studies calculated by Gardner and co-workers used time - differential perturbed angular correlation spectroscopy, (PAC), to study the behaviour of oxygen vacancies trapped by ^{111}In and ^{111}Cd (the daughter isotope) probe defects.

For PAC studies, minute traces of the radioactive isotope ^{111}In are introduced into the host lattice by doping the solution from which the CeO_2 is precipitated. The decay of the probe nucleus to ^{111}Cd is accompanied by the emission of two γ rays. They are emitted consecutively and at a specific angle relative to each other. A perturbation of this angle is a result of the electric field in the lattice around the probe nucleus. Hence, measurement of the angular perturbation can give insight into the electromagnetic field around the probe atom and consequently the lattice environment.

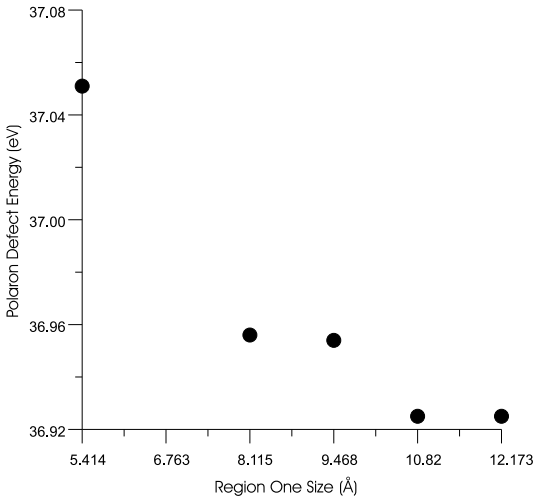

Figure 3.1: The defect energy for a small polaron as a function of region size.

In the present chapter, we consider the binding of these probes to oxygen vacancies. Given this, we go on to study more complex defect clusters which may exist as minority defects or through the exploitation of ceria's range of stoichiometry.

3.2 Methodology

3.2.1 Simulation Techniques

The Mott - Littleton techniques used have been previously discussed in chapter two. The region I and IIa sizes were set to be 10.82Å and 20.00Å respectively. The region sizes were chosen to be large enough to ensure no appreciable change in defect formation energy if the region size is increased further (Figure 3.1).

Interaction	A (eVÅ^{-1})	ρ (Å^{-1})	C (eVÅ^6)
$O^{2-} - O^{2-}$	22764.3	0.149	43.83
$Ce^{4+} - O^{2-}$	1986.8	0.3511	20.40
$Ce^{3+} - O^{2-}$	1731.62	0.3637	14.43
$Cd^{2+} - O^{2-}$	1725.99	0.3497	13.91
$In^{3+} - O^{2-}$	1725.99	0.3442	4.33

Shell Parameters		
	Y (e)	k (eVÅ^{-2})
O^{2-}	-6.10	419.9
Ce^{4+}	7.7	291.8
Ce^{3+}	7.7	291.8
Cd^{2+}	-6.1	840.00
In^{3+}	-6.1	1680.00

Table 3.1: The Potential Parameters

3.2.2 Potential Parameters

The A and ρ parameters for CeO_2 were taken from the work of Butler *et al* [11], the C_6 term was added later to improve the fit to the lattice parameter. The modified potential has been used successfully in subsequent studies, [26, 104]. The values of the parameters along with their shell charges are listed in Table 3.1. The Ce^{3+} - O^{2-}, In^{3+} - O^{2-} and Cd^{2+} - O^{2-} potentials were derived using the empiricisation techniques mentioned in the previous chapter.

3.3 Perfect Cerium Dioxide

Table 3.2 compares the calculated and experimental values for the crystal structure, dielectric and elastic constants of CeO_2. From this it is clear that the potential parameters are able reproduce the experimental data. In particular, the incorporation of the new 'C_6' term improves the fit to the lattice parameters compared with the original potential [11]. In addition, there is an excellent agreement between the calculated and experimental values for the dielectric constants. The agreement between the calculated and experimental elastic constants is not as good. For example the

Property	Calculated	Experiment
Lattice Parameter ($\mathring{A}$)	5.411	5.411
Dielectric Constant		
ϵ_0	19.53	18.6 - 20.0
ϵ_∞	4.00	4.0
Elastic Constant ($x10^{11} Dynescm^{-2}$)		
C_{11}	50.45	40.3 [105]
C_{12}	14.31	10.5
C_{44}	1.61	6.0

Table 3.2: Calculated and experimental values for various properties of CeO_2

calculated C_{11} and C_{12} values are approximately 20 - 25 % higher than the experimental values, which is typical of this type of model. However the calculated C_{44} value is significantly lower than the experimental value. The removal of the C_6 term from the potential does not have a significant effect on the C_{44} and its addition is not a reason for the low value; its removal raises the value only to 2.24 $x10^{11}$ Dynes cm^{-2}.

3.4 Intrinsic Disorder

The sources of intrinsic disorder in stoichiometric CeO_2 are

$$2O_O^X + Ce_{Ce}^X \rightarrow 2V_O^{\bullet\bullet} + V_{Ce}^{||||} + CeO_2 \tag{3.1}$$

$$O_O^X \rightarrow V_O^{\bullet\bullet} + O_i^{||} \tag{3.2}$$

$$Ce_{Ce}^X \rightarrow V_{Ce}^{||||} + Ce_i^{\bullet\bullet\bullet\bullet} \tag{3.3}$$

$V_O^{\bullet\bullet}$	$V_{Ce}^{\prime\prime\prime\prime}$	$O_i^{\prime\prime}$	$Ce_i^{\bullet\bullet\bullet\bullet}$	Schottky Energy per defect	Anion Frenkel Energy per defect	Cation Frenkel Energy
16.06	83.52	-10.43	-65.80	3.33	2.81	8.86

Table 3.3: Disorder reaction energies (in eV)

which are the Schottky, Anion Frenkel, and Cation Frenkel defect mechanisms respectively. The energies for the individual defects, as well as the reaction enthalpies are listed in Table 3.3.

From the tables it can be seen that the likelihood of cation Frenkel defects forming is remarkably low. The Schottky defect energy (E_S) is higher than the anion Frenkel energy (E_F), which would be expected from our current understanding of CeO_2; in that E_S - $2E_F > 0$ [27], which implies that $[V_{Ce}^{\prime\prime\prime\prime}] << [O_i^{\prime\prime}]$. Hence, the most likely form of intrinsic disorder is anion Frenkel. However, this energy is still quite high, thus such disorder will be swamped by the effect of non-stoichiometry in CeO_2. This effect is dicussed further on in this chapter.

3.5 Cadmium and Indium Defects in Stoichiometric Ceria

The charge compensation mechanism for doping with $^{111}In^{3+}$ or $^{111}Cd^{2+}$ is the formation of oxygen vacancies. These can be expressed as,

$$In_2O_3 + 2Ce_{Ce}^X + 4O_O^X \rightarrow 2In_{Ce}^{\prime} + V_O^{\bullet\bullet} + 3O_O^X + 2CeO_2 \tag{3.4}$$

and for the daughter product, cadmium,

$$CdO + Ce_{Ce}^X + 2O_O^X \rightarrow Cd_{Ce}^{\prime\prime} + V_O^{\bullet\bullet} + O_O^X + CeO_2 \tag{3.5}$$

The resulting defects have a Coulombic attraction and may form bound defect clusters. The binding energy of such defect clusters can be given by the expression

$$BE_{Cluster} = \left(\sum_{Comp} E_{Defect} \right) - E_{Cluster} \tag{3.6}$$

therefore a positive binding energy indicates a preference for the cluster over its components. However, with respect to a defect energy the converse is true. A positive defect energy implies energy is required to form the defect. Thus a point defect or defect cluster with the lowest defect energy will be preferred.

3.5.1 Clusters containing a single oxygen vacancy

The defect clusters that we consider consist of either a Cd^{2+} or an In^{3+} ion substituting for a Ce^{4+} lattice ion and an adjacent $V_O^{\bullet\bullet}$. Figure 3.2 illustrates the locations of an oxygen vacancy in the first, second, and third nearest neighbour sites with respect to the impurity ion. The binding and defect energies of the substitutional ion with the oxygen vacancy are listed in Table 3.4. In the case of the Cd^{2+} ion, the binding energy of the vacancy decreases as a function of distance from the cation site. Since the cluster is charge neutral this position preference is clearly being dominanted by the electrostatic attraction between the defects. This belief is justified further when one compares the ionic radii of Ce^{4+} and Cd^{2+}, which are quite similar, 0.97Å and 1.10Å in the octahedral environment [106] respectively. Thus the site preferences cannot be attributed to size effects.

The third nearest neighbour site in the In^{3+} is very unfavourable, however the first and second sites have a very similar binding energy, converse to that seen for the Cd^{2+}

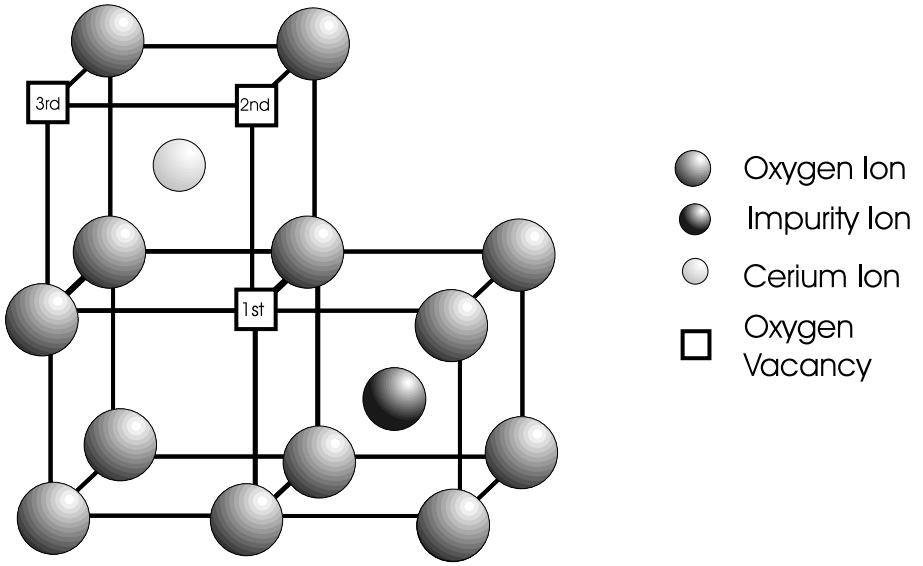

Figure 3.2: First, second, and third neighbour oxygen ion lattice sites with respect to a substitutional ion at (000).

ions. The equality of these sites is a consequence of a competition between the relaxation effect and the Coulombic interactions. Clearly the electrostatic effects would favour the first nearest neighbour site. This is supported by the unrelaxed defect energies; first neighbour, 59.69eV and second nearest neighbour, 65.13eV. However the energy gained when the ions are allowed to relax, the relaxation energy (Unrelaxed Defect Energy - Relaxed Defect Energy), favours the second neighbour site. The relaxation energy of the first neighbour site is 11.26eV while that of the second site is 16.64eV. Thus any Coulombic advantage of the first neighbour site is off set by its lower relaxation energy.

The greater relaxation energy for the second site is a consequence of the fluorite structure. During relaxation, the Ce^{4+} (Figure 3.2) ion adjacent to the oxygen vacancy relaxes away from it due to the latter having an effective positive charge. However, this Ce^{4+} ion is also attracted to the impurity ion, which has an effective

Position of $V_O^{\bullet\bullet}$	Dopant ion at (0, 0, 0)	
	Cd^{2+}	In^{3+}
First neighbour $(1, 1, 1)$	1.14	0.44
Second neighbour $(1, 1, 3)$	0.88	0.42
Third neighbour $(1, 3, 3)$	0.31	0.10

Table 3.4: Binding energies (in eV) of a single oxygen vacancy to substitutional ion.

negative charge. When the vacancy is at the first neighbour position, relaxation away from the vacancy forces it additionally to relax away from the In^{3+} species. In the case of the vacancy at the second site, this is not the case. In fact relaxation of the Ce^{4+} ion away from the vacancy is reinforced by attraction to the In^{3+} ion. This is not merely a size effect, as both the In^{3+} and Ce^{4+} ions are a very similar size, 0.92Å and 0.97Å respectively. Such an effect is not seen for the Cd^{2+} ions as the 2+ charge ensures that Coulombic forces will always dominate.

When the above is applied to PAC experiments, it implies that the fraction of the first and second neighbour indium clusters should be comparable. However when the ^{111}In probe ion decays to ^{111}Cd the second neighbours should jump to first neighbour sites. Experimentally this is observed at temperatures between 100°C and 150°C. Below this temperature the activation barrier to vacancy hopping makes the phenomena too slow to be observed. Wang *et al* estimate the jump barrier to be of the order 0.4 - 0.5 eV, which is close to the calculated value of 0.32eV [107].

3.5.2 Clusters containing two oxygen vacancies

A defect cluster consisiting of a substitutional ion and two nearby oxygen vacancies may be considered as single vacancy cluster (similar to that above) with a second oxygen vacancy bound to it. If the first oxygen vacancy is assumed to be in a first nearest neighbour site the second vacancy can be considered to be at any of the nearest neighbour sites shown in Figure 3.2. The three possibilities are designated: 1st:1st, 1st:2nd and 1st:3rd. It is then possible to consider more complicated situations when the bound cluster vacancy is at a 2nd neighbour site; the 2nd:2nd configurations. The cluster geometries are shown in Figures 3.3 and 3.4 . In all cases the second vacancy can be placed at a number of sites to satisfy the designated criteria. All the appropriate binding energies of the second oxygen vacancy to the defect cluster are listed in Table 3.5.

We first consider the cadmium containing clusters. The Coulombic repulsion between the two negatively charged vacancies results in the preferred positions of the second vacancy to be as far away from the first position within each designated class. However, as the distances between the vacancies increases, the preferences between the furthest and second furthest site become smaller. Consequently in the case of the 2nd:2nd set of clusters there is a negligible preference for the (-1, 1, -3) position over the further away (-1, -1, -3) (0.07eV). Such behaviour can be attributed to the fact that the electrostatic term falls away as 1/r, hence the energy difference of the second vacancy being at (-1, 1, -3) and it being at (-1, -1, -3) sites, will not be as great as the energy difference of the second vacancy at a (1 3 1) site compared with it being at the (-1, 3, 1) position (0.28eV).

Even in the most favoured positions, for all classes, the binding energy of the

Position of both oxygen vacancies	Dopant ion at (000)	
	Cd^{2+}	In^{3+}
$< 1st : 1st >$		
$(1,1,1) : (1,1,-1)$	-0.27	-1.23
$(1,-1,-1)$	0.44	-0.45
$(-1,-1,-1)$	0.57	-0.25
$< 1st : 2nd >$		
$(1,1,1) : (1,3,1)$	-0.97	-1.37
$(1,3,-1)$	-0.05	-0.49
$(-1,3,-1)$	0.15	-0.41
$(1,-3,-1)$	0.15	-0.45
$(1,-3,-1)^a$	0.39	-0.31
$(-1,-3,-1)$	0.43	-0.05
$< 1st : 3rd >$		
$(1,1,1) : (1,3,3)$	-0.57	-0.75
$(-1,3,3)$	-0.41	-0.58
$(1,3,-3)^a$	-0.17	-0.39
$(-1,3,-3)^a$	-0.19	-0.39
$(1,-3,-3)$	-0.07	-0.33
$(-1,-3,-3)$	-0.03	-0.28
$< 2nd : 2nd >$		
$(1,1,3) : (1,-1,3)$	-0.92	-1.37
$(1,3,1)$	-0.02	-0.49
$(-1,3,1)$	0.26	-0.27
$(1,-3,1)^a$	0.49	-0.05
$(-1,-3,1)^a$	0.46	-0.06
$(1,-3,-1)$	0.37	-0.12
$(-1,-3,-1)$	0.50	0.02
$(1,1,-3)$	0.30	-0.17
$(-1,1,-3)$	0.53	0.05
$(-1,-1,-3)$	0.46	-0.03

Table 3.5: Binding energies (in eV) of a second oxygen vacancy to the pre-existing ($M_{Ce} : V_O^{\bullet\bullet}$) defect cluster; ^{a} These binding energies were determined using a region size of $3.5a_0$ (9.47Å) instead of $4.0a_0$ (10.82Å), due to computational difficulties imposed by the low symmetry of the clusters.

second vacancy to the cluster is considerably lower than the binding energy of the first vacancy to the metal ion. Clearly, this would be expected as a result of the Coulombic repulsion between the vacancies. Nevertheless, the detailed situation is more complex, particularly in the case of the 1st:3rd clusters, where the binding energy is unfavourable or zero in all cases. Overall, the most favourable cluster is the 1st:1st cluster where both of the vacancies are diagonally opposite to each other. This particular configuration is seen in the hyperfine experiements of Wang *et al* [102, 103].

In the case of the In^{3+} clusters, the binding energies are negative or close to zero, indicating that at best the second vacancy is not attracted to the cluster and at worst is actually repelled by the cluster. This is not surprising given that the $(In'_{Ce} : V_O^{\bullet\bullet})^{|}$ cluster has an overall negative charge. However, given the relative stability of a single vacancy at a second neighbour site, the results suggest that another vacancy may reside at other second neighbour sites and possibly a first neighbour site with little or no energy penalty. As in the case of the cadmium clusters; the two oxygen vacancies will prefer to be orientated as far apart from each other as possible.

The hyperfine experiments of Wang *et al* [103, 102], show evidence of the formation of the di-vacancy indium cluster . When the dopant concentration is very dilute, the spectra show evidence of a single di-vacancy configuration. If the vacancy concentration is increased by yttrium doping or annealing in-vacuo, two di-vacancy clusters are evident; the symmetric first neighbour configuration and another non-symmetric configuration. These results are in partial agreement with the simulations. The calculations suggest that it is not unfavourable to form *certain* di-vacancy indium clusters. Thus such clusters may be seen experimentally, but not in any significant number, as they form by chance. The experimental evidence suggests this is not the case, and

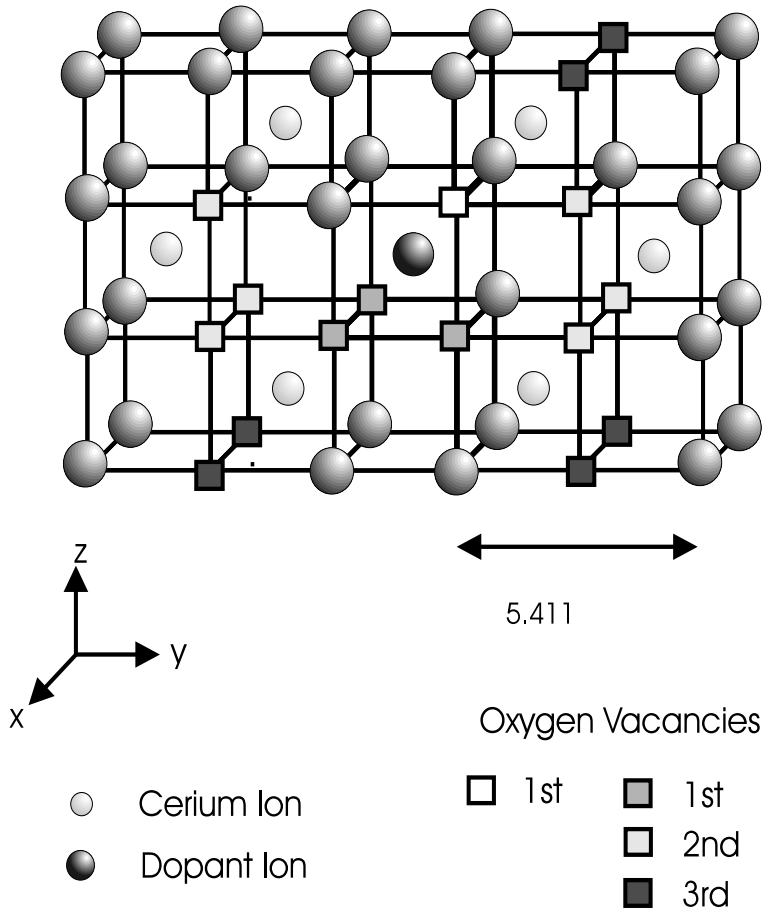

Figure 3.3: Unique defect cluster configurations for a substitutional ion (at (000)), and two oxygen vacancies whose locations are: 1st:1st; 1st:2nd; and 1st:3rd.

that significant amounts of this cluster are seen, which suggests that they do not occur randomly. Nevertheless, both the simulations and experiments do suggest that the two most stable first neighbour di-vacancy clusters are the symmetric $< 111 >$ configuration, and a 1st:2nd configuration. It is therefore possible that we underestimate the binding energy of the second oxygen vacancy.

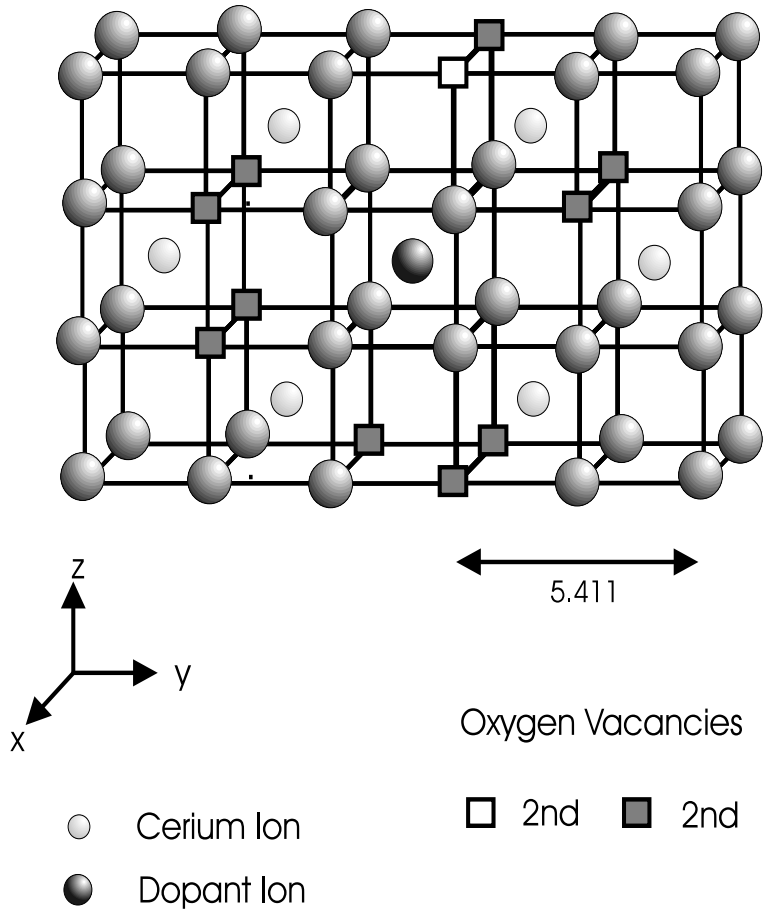

Figure 3.4: Unique defect cluster configurations for a substitutional ion (at (000)), and two oxygen vacancies whose locations are 2nd:2nd.

3.5.3 Defect clusters containing two cation dopants

Since much larger clusters will be considered in the present section, the possible number of defect configurations is prohibitively large. Hence in this and subsequent arrangements, all the defects are placed as far apart from each other as possible within the designated neighbour shell. This method is justified by the results in the previous section. Given this, the combination of the first and second neighbour cation sites *with respect to the oxygen vacancy* results in four possible configurations (Table 3.6). Furthermore, within these constraints there are 4 possible permutations for the metal ions in the defect clusters: $(In_{Ce}^{|} : V_O^{\bullet\bullet} : In_{Ce}^{|})^X$, $(In_{Ce}^{|} : V_O^{\bullet\bullet} : Cd_{Ce}^{||})^|$, $(Cd_{Ce}^{||} : V_O^{\bullet\bullet} : In_{Ce}^{|})^|$, and $Cd_{Ce}^{||} : V_O^{\bullet\bullet} : Cd_{Ce}^{||})^{||}$.

Consider the clusters incorporating two In^{3+} dopants. By comparing the total energies and the binding energies in Table 3.6, it is clear that all the configurations are equally favourable with the exception of when both the dopants are at first nearest neighbour sites. The table shows the binding energy of the second In^{3+} ion is 75% of that for the first ion, implying the second ion is quite strongly bound to the cluster. Figure 3.5 shows the arrangement of the ions when one of the In^{3+} ions is at a second site while the other is at the first nearest neighbour site. The favourability of this 1st:2nd configuration over the 1st:1st configuration is due to a reduction of the electrostatic repulsion as the cation-cation distances are larger.

When both the cations are Cd^{2+} dopants, the situation is analogous to that of the di-In^{3+} cluster. The presence of a second cadmium ion does not destabilise the cluster and actually increases the stability of the charged cluster. The effect of the Coulombic forces is more noticeable in the present set of configurations. The configuration when the Cd^{2+} ions are furthest apart shows a significantly lower binding energy than any

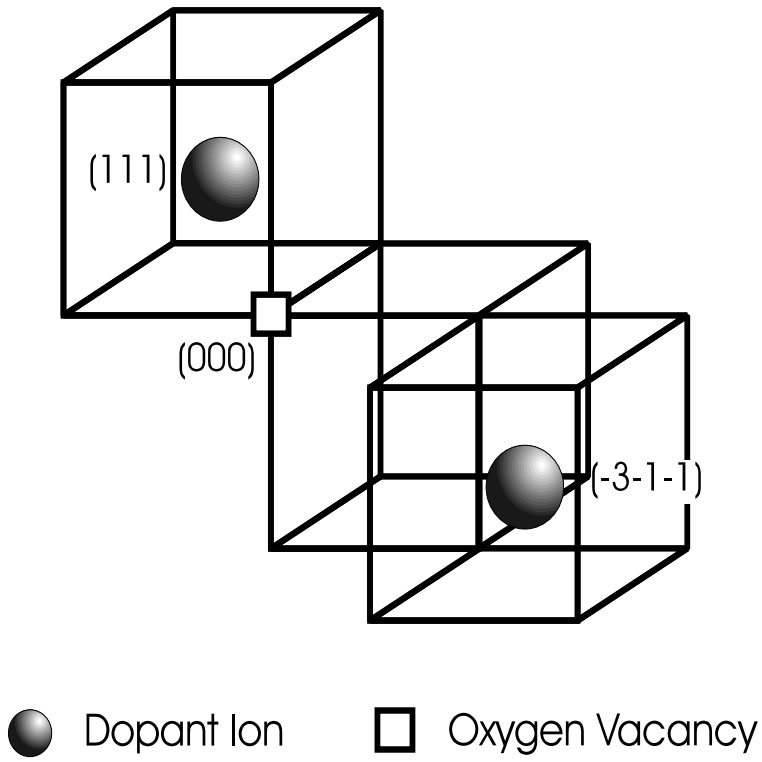

Figure 3.5: Example of a neutral di-In^{3+}:oxygen vacancy cluster, $(In^{|}_{Ce}(1,1,1) : V_O^{\bullet\bullet}(000) : In^{|}_{Ce}(-3,-1,-1))^X$.

of the other configurations.

If a mixed cluster is formed, Table 3.6 shows the most favourable configuration is that where the cadmium dopant is at a first nearest neighbour site and the indium ion is at a second nearest neighbour site. This is a result of the more favourable Coulombic attraction between the Cd^{2+} ions and the $V_O^{\bullet\bullet}$. Such behaviour is similar to the geometry preferences expressed in the single cation clusters.

Cluster	Position of dopant	Total defect energy	Binding Energy of second cation
	$In^{\prime}_{Ce}$		
$(In^{\prime}_{Ce}(1,1,1) : V_O^{\bullet\bullet})^{\bullet}$	(-1,-1,1)	80.88	0.20
$(In^{\prime}_{Ce}(1,1,1) : V_O^{\bullet\bullet})^{\bullet}$	(-3,-1,-1)	80.76	0.33
$(In^{\prime}_{Ce}(3,1,1) : V_O^{\bullet\bullet})^{\bullet}$	(-1,-1,1)	80.76	0.33
$(In^{\prime}_{Ce}(3,1,1) : V_O^{\bullet\bullet})^{\bullet}$	(-3,-1,-1)	80.76	0.32
	$Cd^{\prime\prime}_{Ce}$		
$(In^{\prime}_{Ce}(1,1,1) : V_O^{\bullet\bullet})^{\bullet}$	(-1,-1,1)	107.36	0.76
$(In^{\prime}_{Ce}(1,1,1) : V_O^{\bullet\bullet})^{\bullet}$	(-3,-1,-1)	107.41	0.71
$(In^{\prime}_{Ce}(3,1,1) : V_O^{\bullet\bullet})^{\bullet}$	(-1,-1,1)	107.14	1.00
$(In^{\prime}_{Ce}(3,1,1) : V_O^{\bullet\bullet})^{\bullet}$	(-3,-1,-1)	107.45	0.69
	$In^{\prime}_{Ce}$		
$(Cd^{\prime\prime}_{Ce}(1,1,1) : V_O^{\bullet\bullet})^{X}$	(-1,-1,1)	107.36	0.00
$(Cd^{\prime\prime}_{Ce}(1,1,1) : V_O^{\bullet\bullet})^{X}$	(-3,-1,-1)	107.41	0.23
$(Cd^{\prime\prime}_{Ce}(3,1,1) : V_O^{\bullet\bullet})^{X}$	(-1,-1,1)	107.14	0.22
$(Cd^{\prime\prime}_{Ce}(3,1,1) : V_O^{\bullet\bullet})^{X}$	(-3,-1,-1)	107.45	0.18
	$Cd^{\prime\prime}_{Ce}$		
$(Cd^{\prime\prime}_{Ce}(1,1,1) : V_O^{\bullet\bullet})^{X}$	(-1,-1,1)	133.94	0.49
$(Cd^{\prime\prime}_{Ce}(1,1,1) : V_O^{\bullet\bullet})^{X}$	(-3,-1,-1)	133.82	0.61
$(Cd^{\prime\prime}_{Ce}(3,1,1) : V_O^{\bullet\bullet})^{X}$	(-1,-1,1)	133.82	0.61
$(Cd^{\prime\prime}_{Ce}(3,1,1) : V_O^{\bullet\bullet})^{X}$	(-3,-1-1)	134.25	0.18

Table 3.6: Formation of clusters with two substitutional ions adjacent to an oxygen vacancy at (000). All energies eV.

3.6 Defects in non-stoichiometric ceria

It has been established that the electron conduction in CeO_2 proceeds via a localised small polaron hopping mechanism [4, 6]. A polaron in the context of the ionic model is a Ce^{3+} ion. Additionally, it is well known that CeO_2 exhibits a broad range of stoichiometries, CeO_{2-x}, where x $\leq$ 0.28 [4]. Thus, in the present section we consider the energetics of polaron binding to oxygen vacancies and their associated Cd^{2+} and In^{3+} substitutional defects.

The reduction of CeO_2 can be written as,

$$2Ce_{Ce}^{x} + O_{O}^{x} \rightarrow 2Ce_{Ce}^{|} + V_{O}^{\bullet\bullet} + \frac{1}{2}O_2(g) \tag{3.7}$$

Table 3.7 shows the enthalpy of this reaction to be 6.51eV. The energy to create a $V_O^{\bullet\bullet}$ via the Frenkel mechanism is 5.6eV. However, there are two factors which make the reduction of CeO_2 more energetically favourable than Frenkel disorder. The first is the increase in configurational entropy resulting from the formation of an O_2 gas molecule. This lowers the reaction energy by 1.2eV at 1000K and 1 atm pressure [72], thus the energy of equation 3.7 becomes 5.31eV. Of course there is an entropy term with the anion Frenkel reaction but this will be much smaller at comparable temperatures and pressures. The second factor is the formation of defect clusters which makes the reduction process more favourable by approximately 0.9eV (Table 3.8). Therefore, the overall reaction energy is reduced to 4.41eV. This is by far the lowest of the disorder mechanisms discussed. Hence non-stoichiometry will tend to be responsible for producing the majority of the defect species in CeO_2.

Reaction	Energy (eV)	Process
$Ce_{\infty}^{4+} + 1e^{-} \rightarrow Ce_{\infty}^{3+}$	-36.76	Electron affinity
$Ce_{\infty}^{3+} \rightarrow Ce_{Ce}^{\cdot}$	36.93	CASCADE Defect energy
$O_O^X \rightarrow V_O^{\bullet\bullet} + O_{\infty}^{2-}$	16.06	CASCADE Defect energy
$O_{\infty}^{2-} \rightarrow O_{\infty}^{-} + 1e^{-}$	-8.8	2nd Electron affinity
$O_{\infty}^{-} \rightarrow O_{\infty} + 1e^{-}$	1.466	1st Electron affinity
$O_{\infty} \rightarrow \frac{1}{2}O_{2(g)}$	-2.558	Molecular dissociation
Overall reaction energy	6.51eV	

Table 3.7: Born-Haber cycle for equation 3.7

Cluster	Position of $Ce_{Ce}^{\cdot}$	Total defect energy	Polaron binding energy
$V_O^{\bullet\bullet}$	(1,1,1)	52.58	0.36
$V_O^{\bullet\bullet}$	(3,1,1)	52.50	0.43
$(Ce_{Ce}^{\cdot}(1,1,1) : V_O^{\bullet\bullet})^{\bullet}$	(-1,-1,1)	89.30	0.20
$(Ce_{Ce}^{\cdot}(1,1,1) : V_O^{\bullet\bullet})^{\bullet}$	(-3,-1,-1)	89.03	0.47
$(Ce_{Ce}^{\cdot}(3,1,1) : V_O^{\bullet\bullet})^{\bullet}$	(-1,-1,1)	89.03	0.40
$(Ce_{Ce}^{\cdot}(3,1,1) : V_O^{\bullet\bullet})^{\bullet}$	(-3,-1,-1)	89.05	0.38

Table 3.8: Binding energies (in eV) of a polaron to a single oxygen vacancy at (000) to form $(Ce_{Ce}^{\cdot} : V_O^{\bullet\bullet})^{\bullet}$ and $(Ce_{Ce}^{\cdot} : V_O^{\bullet\bullet} : Ce_{Ce}^{\cdot})^X$clusters.

3.6.1 Defect clusters in undoped ceria

The binding energies and defect energies that describe defect clusters in undoped CeO_{2-x} are reported in Table 3.8. The origin, as with the work described in Table 3.6, is centred on the $V_O^{\bullet\bullet}$. Two single polaron trap sites are considered, the resulting geometries are equivalent to the first and second nearest neighbour sites discussed in section 3.5.1 and in Figure 3.2. The situation is analogous to that for the In^{3+} ion, both the trap sites have energies close to each other, in fact the second neighbour site is slightly more favourable, as a result of the Ce^{3+} atom being slightly larger than an In^{3+}, 1.14Å and 0.92Å respectively [106].

The difference in the formation enthalpies between a singly and doubly charged oxygen vacancy has been determined to be 0.56eV [6]. In the present model this corresponds to a binding energy of a single polaron to an oxygen vacancy. Consequently, it is clear that the calculations are in close accord with the experimental data.

For two polaron systems the combination of first and second nearest neighbour sites results in four configurations, the same as those seen in section 3.5.3 and Figure 3.5 . The results in Table 3.8 show an analogous situation to that seen for the $(In^{|}_{Ce} : V^{\bullet\bullet}_{O} : In^{|}_{Ce})^{X}$ clusters with the least favourable geometry being that where both the polarons are at first neighbour sites. The total defect energy in Table 3.8 shows quite a significant energy difference between this configuration and the other second neighbour containing configurations which have similar energies, approximately 0.3eV.

The binding energy of the second polaron to the single polaron cluster, $(Ce^{|}_{Ce} : V^{\bullet\bullet}_{O})^{\bullet}$ is 0.4eV. This binding energy is approximately the same magnitude as that of the first polaron to the vacancy. This second polaron is highly favourable as it results in the formation of a neutral cluster. In general, the magnitude of the binding energies are close to those of the $(In^{|}_{Ce} : V^{\bullet\bullet}_{O} : In^{|}_{Ce})^{X}$ clusters, as one would expect, given their Coulombic parity.

3.6.2 Binding of polarons to $(In^{|}_{Ce} : V^{\bullet\bullet}_{O})^{\bullet}$ and $(Cd^{||}_{Ce} : V^{\bullet\bullet}_{O})^{X}$ clusters

Table 3.9 shows that when the substitutional ion is In^{3+} the situation mirrors that concerning the trapping of two polarons to an oxygen vacancy. Thus the arrangement when both the polaron and the In^{3+} are in first nearest neighbour sites is the

		Total defect energy		Polaron binding energy	
Cluster	Position of dopants	Cd	In	Cd	In
$(Ce^{\downarrow}_{Ce}(111) : V_O^{\bullet\bullet})$	(-1-11)	111.54	85.08	0.07	0.21
$(Ce^{\downarrow}_{Ce}(111) : V_O^{\bullet\bullet})$	(-3-1-1)	111.22	84.86	0.40	0.43
$(Ce^{\downarrow}_{Ce}(311) : V_O^{\bullet\bullet})$	(-1-11)	111.54	84.94	0.35	0.35
$(Ce^{\downarrow}_{Ce}(311) : V_O^{\bullet\bullet})$	(-3-1-1)	111.60	84.90	0.29	0.39

Table 3.9: Binding energies (in eV) of a single oxygen vacancy to substitutional ion.

least favourable of the four configurations, while the other three configurations have comparable energies.

If the impurity ion is Cd^{2+}, the defect cluster is neutral and one would expect the binding of a polaron to be unfavourable. However, the binding energy of the polaron to the cluster is comparable with the $(In^{\downarrow}_{Ce} : V_O^{\bullet\bullet} : Ce^{\downarrow}_{Ce})^X$ cluster, when either the Cd^{2+} ion or the polaron are at second neighbour sites.

3.6.3 Binding of a polaron to a $(V_O^{\bullet\bullet} : M_{Ce} : V_O^{\bullet\bullet})$ cluster

We consider the possibilities of polaron trapping to the two vacancy metal clusters discussed in section 3.5.2. The results in Table 3.10 suggest if the cation is indium, the di-vacancy cluster will bind strongly to a polaron. The most stable double vacancy cluster has an energy of 0.57eV. This stable trap site is, once again, when the polaron is at a second neighbour site. However, if In^{3+} is already at second site with respect to the vacancy the polaron can reside at a first neighbour site with no energy penalty.

If the cation is Cd^{2+}, the double oxygen vacancy cluster will also strongly trap a polaron. The trapping energies in this case are only slightly less than those for the In^{3+} clusters. The most stable second neighbour trap site is shown in Figure 3.6 .

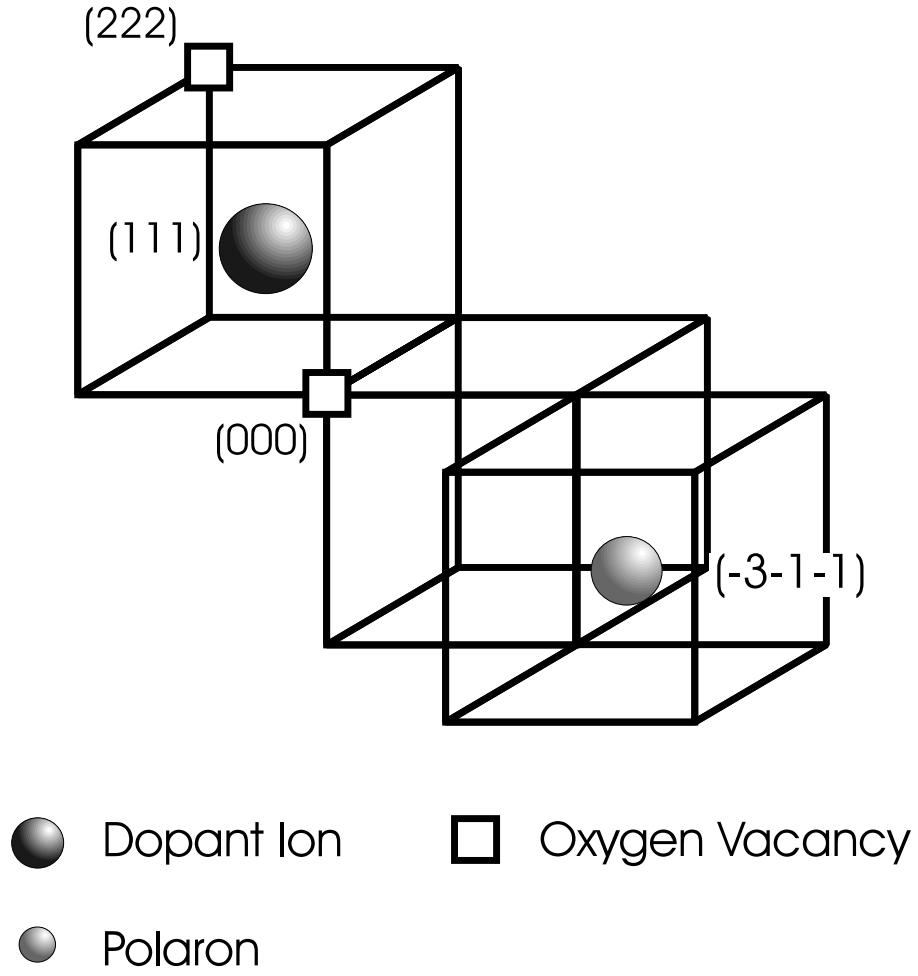

Figure 3.6: The most stable arrangement of the $(Ce^{\perp}_{Ce}(-3,-1,1) : V_O^{\bullet\bullet}(0,0,0) : Cd^{\parallel}_{Ce} : V_O^{\bullet\bullet}$ (2,2,2))$^{\bullet}$ defect cluster.

		Total defect energy		Polaron binding energy		Binding energy with respect to $(M_{Ce} : V_O^{\bullet\bullet})$ and $(Ce_{Ce}^{\mid} : V_O^{\bullet\bullet})$ clusters	
Cluster	Position of $Ce_{Ce}^{\mid}$	Cd	In	Cd	In	Cd	In
$(V_O^{\bullet\bullet} : M_{Ce}(1,1,1) : V_O^{\bullet\bullet}(2,2,2))$	(-1,-1,1)	126.97	101.32	0.27	0.39	0.29	-0.38
$(V_O^{\bullet\bullet} : M_{Ce}(1,1,1) : V_O^{\bullet\bullet}(2,2,2))$	(-3,-1,-1)	126.69	101.14	0.55	0.57	0.49	-0.27
$(V_O^{\bullet\bullet} : M_{Ce}(1,1,1) : V_O^{\bullet\bullet}(4,2,2))$	(-1,-1,1)	127.28	101.29	0.47	0.49	-0.03	-0.35
$(V_O^{\bullet\bullet} : M_{Ce}(1,1,1) : V_O^{\bullet\bullet}(4,2,2))$	(-1,-1,1)	127.34	101.29	0.47	0.49	-0.03	-0.35
$(V_O^{\bullet\bullet} : M_{Ce}(3,1,1) : V_O^{\bullet\bullet}(6,2,2))$	(-1,-1,1)	127.74	101.66	0.43	0.45	-0.21	-0.72
$(V_O^{\bullet\bullet} : M_{Ce}(3,1,1) : V_O^{\bullet\bullet}(6,2,2))$	(-3,-1,-1)	128.13	101.96	0.04	0.15	-0.67	-1.09

Table 3.10: Formation of $(Ce_{Ce}^{\mid} : V_O^{\bullet\bullet} : M_{Ce} : V_O^{\bullet\bullet})$ clusters, energies in eV.

3.6.4 Binding of $(In^{|}_{Ce} : V_O^{\bullet\bullet})^{\bullet}$ and $(Cd^{||}_{Ce} : V_O^{\bullet\bullet})^{X}$ clusters to the $(Ce^{|}_{Ce} : V_O^{\bullet\bullet})^{\bullet}$ cluster

The large defect clusters considered in the previous section can be considered as consisiting of smaller pairs of defects. These binding energies are show (Table 3.10), when the dopant ion is In^{3+} the larger clusters are markedly unstable with respect to the smaller defect clusters. Thus, the binding of the polaron to the double cluster actually makes it unstable and would make this cluster geometry unlikely to exist. If the impurity ion is Cd^{2+} the most stable configurations are also stable with respect to dissociation, with the other favourable configurations having almost zero binding energy with respect to dissociation.

3.7 Summary

The simulations suggest that in general, the Cd^{2+} prefers to be at a first nearest neighbour site with respect to the oxygen vacancy. However, for the In^{3+} the situation is more complex. For a single In^{3+} ion, the dopant exhibits an equal predisposition to either the first or second nearest neighbour site. For clusters involving polarons the Ce^{3+} ion behaves like the In^{3+} dopant, showing a preferrence for the second neighbour site.

Clusters involving two oxygen vacancies will form if the associated cation is cadmium but are unstable or at best show zero binding energy for the second vacancy if the cation is In^{3+}. Polaron defects will bind very strongly to such di-vacancy clusters. However, if the dopant ion is In^{3+} , the association of a polaron to the cluster results in it becoming unstable with respect to smaller defect pairs.

One of the important factors with the present work is the synergy between the computer simulation results and the those of the experiements. The simulation provide atomistic interpretations for some of the observations and the experiments in turn provide quantitative verification of some of the simulation predictions.